TU Delft

Delft University of Technology

Document Version
Final published version

Licence
CC BY

Citation (APA)
Fan, J., Steinberg, M., Jahn, A., Cao, C., & Feld, S. (2026). Biased-noise thresholds of zero-rate holographic codes with tensor-network decoding. *Physical Review A*, *114*(1), Article 012447. https://doi.org/10.1103/RCXG-X3HY

Important note
To cite this publication, please use the final published version (if applicable).
Please check the document version above.

Copyright
In case the licence states “Dutch Copyright Act (Article 25fa)”, this publication was made available Green Open Access via the TU Delft Institutional Repository pursuant to Dutch Copyright Act (Article 25fa, the Taverne amendment). This provision does not affect copyright ownership.
Unless copyright is transferred by contract or statute, it remains with the copyright holder.

Sharing and reuse
Other than for strictly personal use, it is not permitted to download, forward or distribute the text or part of it, without the consent of the author(s) and/or copyright holder(s), unless the work is under an open content license such as Creative Commons.

Takedown policy
Please contact us and provide details if you believe this document breaches copyrights.
We will remove access to the work immediately and investigate your claim.

This work is downloaded from Delft University of Technology.

Biased-noise thresholds of zero-rate holographic codes with tensor-network decoding

J. Fan,[1,2,*] M. Steinberg,[1,2,*,†] A. Jahn,[3] C. Cao,[4] and S. Feld[1,2]
[1]*QuTech, Delft University of Technology, 2628 CJ Delft, The Netherlands*
[2]*Quantum and Computer Engineering Department, Delft University of Technology, 2628 CD Delft, The Netherlands*
[3]*Department of Physics, Freie Universität Berlin, 14195 Berlin, Germany*
[4]*Department of Physics, Virginia Tech, Blacksburg, Virginia 24061, USA*

(Received 23 August 2024; revised 27 April 2026; accepted 1 July 2026; published 20 July 2026)

A crucial insight for practical quantum error correction is that different types of errors, such as single-qubit Pauli operators, typically occur with different probabilities. Finding an optimal quantum code under such biased noise is a challenging problem, related to the (generally unknown) maximum capacity of the corresponding noisy channel. A benchmark for this capacity is given by the hashing bound, which describes the performance of random stabilizer codes and leads to the matter of identifying codes that come close to the bound while also being efficiently decodable. In this work, we perform a comprehensive analysis of asymptotically zero-rate holographic codes under biased noise. We show that many representatives from such models of this code class fulfill both the channel optimality and efficient decoding guarantees for tensor-network codes. In fact, all tested holographic codes are found to reach the hashing bound in some bias regime, while several built from the $[\![5, 1, 2]\!]$ surface code and $[\![6, 1, 3]\!]$ code exceed state-of-the-art code performance in the 2-Pauli noise regime. Furthermore, we consider Clifford deformations which allow all considered codes to reach the hashing bound for 1-Pauli noise as well. Our results establish that holographic codes, which were previously shown to possess efficient tensor-network decoders, also exhibit competitive thresholds under biased noise.

DOI: 10.1103/rcxg-x3hy

I. INTRODUCTION

Holographic codes are quantum codes conventionally studied as toy models of the anti–de Sitter/conformal field theory (AdS/CFT) correspondence [1–6], where they have led to remarkable insights in quantum gravity. However, because their relevance in quantum gravity is mostly theoretical [6], comparatively little is known about their practical error-correction capabilities in contrast to leading benchmarks of quantum error correction, such as the surface code. In addition, recent advances in tensor network codes [7] and the quantum LEGO formalism [8] have brought them closer to a practically viable regime. For example, leveraging their flexibility in a modular construction, holographic codes with high encoding rate and greatly exceeding the $O(n^{1/2})$ distance scaling have been proposed [9] alongside schemes for implementing universal fault-tolerant logic based on heterogeneous code constructions [10]. The hyperbolic geometry of holographic codes also implies that such codes admit efficient optimal tensor network decoders for all independent and identically distributed single-qubit errors [11] since their tensor networks can be contracted in polynomial time even without bond truncation. Under such decoders, they have been shown to yield a code capacity threshold that is as high as that of the surface code [7] under depolarizing noise where all Pauli errors occur with equal probability.

Although there remain many open questions before holographic codes can be fairly assessed at a practical level, e.g., determining the fault-tolerant threshold, there are properties that are poorly understood even at the code capacity level, where syndrome extractions are perfect. One such open question is the performance of the code when the error channels are biased. Biased noise is found in many physical quantum devices wherein certain Pauli errors occur more frequently than others, such as phase flips being more likely than bit flips. The presence of bias can also lead to better error correction with superior thresholds and effective distances [12–15]. In certain topological codes (e.g., Clifford-deformed topological codes such as the XZZX surface code), the threshold under biased noise has also been shown to attain the error threshold set by the hashing limit, which sets a target benchmark for good quantum error-correcting codes that can be used for efficient information transmission under a noisy channel. In holographic codes, however, there is very little understanding of their performance against biased errors [11,16].

In this work, we provide a characterization of holographic codes under biased noise. We study common classes of holographic codes and their deformations to demonstrate that asymptotically zero-rate holographic quantum codes admit high code capacity thresholds comparable to leading benchmarks under biased noise and can either achieve or supersede

*These authors contributed equally to this work.
†Contact author: matt.steinberg3@gmail.com

Published by the American Physical Society under the terms of the Creative Commons Attribution 4.0 International license. Further distribution of this work must maintain attribution to the author(s) and the published article's title, journal citation, and DOI.

the hashing bound for various Pauli channels of interest. The possibility of holographic codes as an alternative class of code constructions to exceed the hashing bound is also of independent interest, as a central problem in quantum coding theory is to identify efficiently decodable codes that can attain or even exceed the hashing bound. A class of such codes will not only provide new approaches for obtaining tighter *quantum channel capacity* (QCC) lower bounds, but also inspire proposals for more efficient strategies of error correction [13,17–21].

Using tensor-network decoding techniques from [7,16], we study zero-rate versions of six different classes of holographic codes which are constructed from the seed codes of the following:

(1) $[\![5, 1, 3]\!]$, i.e., Harlow-Preskill-Pastawski-Yoshida (HaPPY) code [5].
(2) Tailored $[\![7, 1, 3]\!]$ code [22].
(3) $[\![7, 1, 3]\!]$ Steane code [23].
(4) $[\![6, 1, 3]\!]$ code [7].
(5) Surface-code fragment (SCF) [24].
(6) A Clifford-deformed variant of the Steane code.

Utilizing the holographic code examples listed, our main results can then be stated as follows:

(1) In the limit of pure 2-Pauli noise channels, the thresholds calculated for zero-rate SCF and $[\![6, 1, 3]\!]$ holographic codes exceed current state-of-the-art results [17,19,20]. To our knowledge, no other class of quantum codes has thus far been able to supersede the hashing limit for pure 2-Pauli noise.

(2) All of the holographic codes tested in the limit of pure 2-Pauli noise either come within 2% of, attain, or overcome some portion of the hashing bound. Furthermore, all tested codes were found to either attain or overtake the hashing bound for some bias configuration of the Pauli noise channel.

(3) We apply the method of *Clifford deformations* from [15,25] to the holographic Steane code, demonstrating that the threshold of the code can be drastically modified for depolarizing, pure-X, and pure-Z noise channels.

Our results provide strong evidence that holographic codes possess high resilience against various types of Pauli noise channels and can be tuned accordingly. In sharp contrast with other code families, maximum-likelihood decoding of holographic codes and the computation of their weight enumerator polynomials are possible in polynomial time, even with exact tensor-network contractions [7,11], further bolstering their practical potential for both quantum error correction and for numerical studies of QCC bounds.

The remainder of this article is organized as follows: Section II reviews holographic codes and tensor-network decoding, Sec. III describes the simulation setup and biased-noise threshold results, and Sec. IV summarizes the implications and open directions.

II. BACKGROUND

A. Holographic quantum error correction

Originally developed to model the AdS/CFT correspondence [1–3,6], holographic quantum error correction involves encoding maps from *bulk* (logical) degrees of freedom on a $d+1$-dimensional hyperbolic space to d-dimensional *boundary* (physical) degrees of freedom. While in full AdS/CFT the bulk and boundary degrees of freedom are associated with weakly coupled quantum gravity on an asymptotically anti–de Sitter (AdS) background and strongly coupled conformal field theory (CFT), respectively, aspects of this duality for $d = 1$ can be captured by simple tensor-network codes [4–6].

Holographic quantum codes are, at their core, generalized concatenated codes [10,26,27], as their treelike concatenation structure is a consequence of the bulk logical qubits being divisible into radial layers [5,28,29]. The most widely studied instances of holographic codes also fall into the category of stabilizer codes [5,23,30], despite some restrictions on their representation of holographic dualities [31] and the possibility to construct more sophisticated nonstabilizer, approximate, or generalized holographic codes [32–34]. We shall therefore limit ourselves to stabilizer versions of holographic codes in the present work.

Stabilizer codes themselves are defined as codes for which the logical operators $\mathcal{L}$ and codeword stabilizers $\mathcal{S}$ consist of elements $P_i \in \mathsf{P}^n$, where P^n is the n-qubit Pauli group, P_i takes the form $P_{i_1} \otimes \cdots \otimes P_{i_n}$, and $P \in \{I, X, Y, Z\}$, i.e., the single-qubit Pauli operators. It is also wholly possible to consider finite-rate versions of holographic codes, wherein individual seed tensors can be specified with logical-qubit implantation. In this work, we consider only zero-rate versions of holographic codes, wherein only the central logical index remains (Fig. 1).

Represented as tensor networks, the bulk geometry of holographic codes is that of a regular hyperbolic tiling, wherein each n-gon tile is filled out by one tensor of n planar (i.e., nonlogical) legs. Starting from the central seed tensor whose single logical leg describes degrees of freedom in a small bulk patch in holography, the tensor network (and the bulk region it represents) can be iteratively extended via inflation steps. Here, each of these extensions can be realized by adding a layer of tensors (contracted) to the tensor network [28,29]. While this process is not unique, we will only apply edge inflation in this work (i.e., tensors or tiles are added to all open legs or edges of the previous step). We denote the number of inflation steps as R, with $R = 0$ describing the seed tensor by itself, with Fig. 1 showing holographic codes on various hyperbolic tilings at $R = 2$.

From a practical perspective, there are many reasons to find the concept of a holographic quantum code appealing. First, holographic codes are relatively simple to construct and scale from small, atomized examples to larger example codes. As a direct consequence of the quantum LEGO formalism [8], concepts such as code structure and transversal logical operations are straightforward to intuit [10,35]. Second, the boundary of holographic codes exhibits a quasiperiodic self-similarity [28,29], allowing one to rescale the number of physical and logical qubits using local inflation rules that also determine the code's rate and distance scaling [9,16], both of which fare better than other constructions [36–39]. Third, it is known that most seed tensors for holographic codes can be easily mapped to graph states, implying that efficient preparation schemes likely exist [40–43]. Lastly, and perhaps most consequentially, it has been shown that holographic codes exhibit high resilience against various noise channels. Indeed, it was first shown in [5] that holographic quantum error-correction

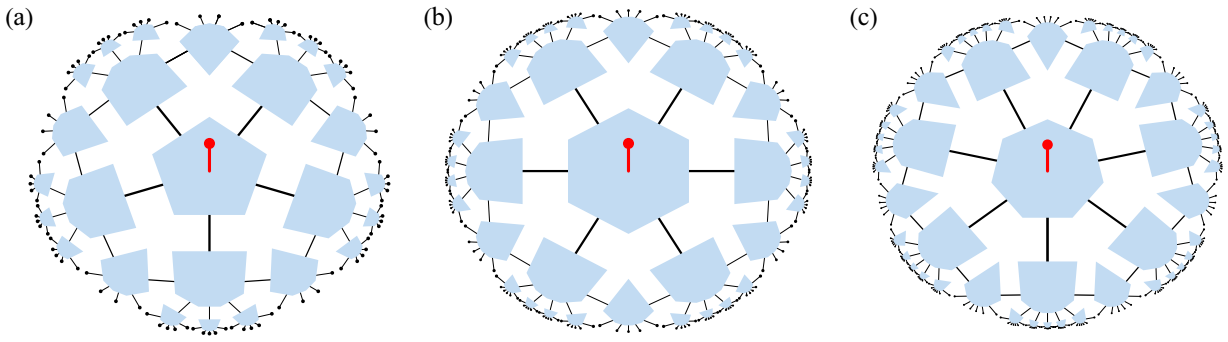


FIG. 1. The holographic tensor-network codes considered in this work: (a) The Harlow-Preskill-Pastawski-Yoshida (HaPPY) code [5] whose pentagon-hexagon geometry also underlies the holographic surface-code fragment (SCF) model [24], (b) the holographic $[\![6, 1, 3]\!]$ code [7], and (c) the holographic Steane code [23]. All are defined as tensor-network contractions of copies of a fixed q-leg tensor on a hyperbolic tiling, with the central tensor used as a *seed tensor* for the encoding isometry of a $[\![q-1, 1, d]\!]$ code with some distance d. The remaining tensors have all q legs contracted in the plane, leading to a larger encoding map between one logical qubit (central red leg) and the boundary physical qubits (open black legs). Here we depict the codes with $R = 2$ layers of edge inflation. In the $R \to \infty$ limit, the rate of each code goes to zero.

codes exhibit high thresholds against the quantum erasure channel; subsequently, several works have shown the capability of certain code constructions to protect against depolarizing and 1-Pauli noise, potentially as well as topological codes [7,9,16,23,24,44]. To our knowledge, a systematic biased-noise threshold study for even zero-rate holographic codes has not been performed, let alone for their constant-rate versions (Ref. [11] discusses biased noise in finite-rate HaPPY pentagon codes, but it only captures the nondetectable error probability for a code of fixed length). As such, our work takes a towards understanding holographic codes under more generalized noise channels.

The main ingredient of a holographic quantum code is the seed tensor, defining the encoding map for a single tile (in Sec. II B, we will provide descriptions of several seed codes which may be unfamiliar to the reader, such as the SCF and the tailored $[\![7, 1, 3]\!]$ codes). Here we consider the zero-rate case with a logical qubit only on the central tile; on the remaining tiles, all tensor legs are planar, effectively dispersing the logical information towards the tiling boundary. Note that in generic holographic codes, each tile may hold a logical qubit, leading to a nonzero asymptotic rate as the number R of layers is increased.

Currently, several methods exist by which one may create a holographic code. First, one may employ methods of gauge fixing for various logical qubits in the bulk. This step leaves each encoding tensor with only physical legs that act isometrically from one layer to the next. In the second case, one can tile the bulk by surrounding a code with parameters $[\![n, k, d]\!]$ by codes with parameters $[\![n+1, 0, d+1]\!]$. In both cases, the contracted tensor network then forms one large encoding isometry from a single logical qubit to the physical boundary qubits given suitable (e.g., *perfect* [5]) tensors. Here, we opt for the second case. Third, copies of the same seed tensor are typically used to construct such codes, but one may also employ several different seed tensors in similar spirit to heterogeneous concatenation methods for tree-style concatenated codes [10,45,46]. We note that for all of these techniques, it was recently shown that holographic codes are an instance of generalized code concatenation [10,27].

B. Seed tensors used in this paper

Here we provide information on the seed codes utilized in this paper: the perfect $[\![5, 1, 3]\!]$ code [47], the Steane code [48], the $[\![6, 1, 3]\!]$ code [49], the surface-code fragment (SCF) from Ref. [24], and the tailored $[\![7, 1, 3]\!]$ code [22].

First, The famous perfect code of [47] is a $[\![5, 1, 3]\!]$ code with cyclically permuted stabilizer support, as shown in Table I. The perfect code is an example of generalized XZZX toric codes [14] and is known to exhibit high resilience against biased 1-Pauli noise [13,22]. Equally famous in its own right, the Steane code is the prototypical example of a Calderbank-Shor-Steane (CSS) code, in which two classical codes are utilized in order to construct a quantum code. The Steane code in particular is a self-dual CSS code, meaning that the X and Z portions of the stabilizer generators are exactly coinciding. More information on both codes can be found in Refs. [26,50], and the stabilizers and logical operators for the code can be found in Table I.

The surface-code fragment (SCF) is the smallest surface code and is known to possess a block-perfect encoding tensor, following the work of Ref. [24]. The stabilizers and logical operators for the SCF seed tensor are shown in Table I. The block-perfect condition is taken to mean that given any cyclic permutation of the SCF tensor indices $\{1, 2, 3, 4, \bar{6}, 5\}$ (where $\bar{6}$ denotes the logical index), we can construct the condition whereby

$$\mathrm{Tr}_A[|\psi\rangle\langle\psi|] \propto \mathbb{I}, \tag{1}$$

where $|A| = \lfloor \frac{n}{2} \rfloor$. The SCF seed tensors are an instance of planar maximally entangled (PME) states [51], meaning that only adjacent groupings into bipartitions can reduce to maximally mixed states.

The tailored $[\![7, 1, 3]\!]$ code is a generalization of the perfect code and was first introduced in [22]. The stabilizers and logical operators for the code are listed in Table I. As stated in [14,52], both the perfect code and the tailored $[\![7, 1, 3]\!]$ codes can be regarded as the smallest toric codes with so-called shifted boundary conditions. The tailored $[\![7, 1, 3]\!]$ code was

TABLE I. Seed tensors and their stabilizers, as well as logical operators for select holographic codes.

Seed tensor	Stabilizers	Logical operators
HaPPY	$XZZXI\bar{I}, IXZZX\bar{I}, XIXZZ\bar{I}, ZXIXZ\bar{I}$	$ZZZZZ\bar{Z}, XXXXX\bar{X}$
Tailored $[\![7, 1, 3]\!]$	$XZIZXII\bar{I}, IXZIZXI\bar{I}, IIXZIZX\bar{I}, XIIXZIZ\bar{I}, ZXIIXZI\bar{I}, IZXIIXZ\bar{I}, ZIZXIIX\bar{I}$	$ZZZZZZZ\bar{Z}, XXXXXXX\bar{X}$
Steane	$XXIIIXX\bar{I}, IXXXIIX\bar{I}, IIIXXXX\bar{I}, ZZIIIZZ\bar{I}, IZZIIZI\bar{I}, IIIZZZZ\bar{I}$	$ZZZZZZZ\bar{Z}, XXXXXXX\bar{X}$
$[\![6, 1, 3]\!]$	$ZIZIII\bar{I}, XZYYXI\bar{I}, XXXXZI\bar{I}, IZZXIX\bar{I}, XYXYIZ\bar{I}$	$XZXZII\bar{X}, XYYXII\bar{Z}$
SCF	$XXIXI\bar{I}, IIXXX\bar{I}, ZIZZI\bar{I}, IZIZZ\bar{I}$	$XIXII\bar{X}, IIZIZ\bar{Z}$
CD-Steane	$XZZIIIX\bar{I}, XIZXZII\bar{I}, XIIIZZX\bar{I}, ZXXIIIZ\bar{I}, ZIXZXII\bar{I}, ZIIIXXZ\bar{I}$	$XZZXZZX\bar{X}, ZXXZXXZ\bar{Z}$

shown in [22] to exhibit better threshold performance than the Steane code in the setting of highly biased noise.

C. Tensor-network decoding

Contracting a tensor network representing a holographic-code state with potentially thousands of qubits is computationally intractable; as such, we follow a simplification technique proposed in Refs. [7,16], briefly reviewed here.

In the tensor-network decoder formalism, we represent stabilizer operators as elements in $\mathbb{Z}_4$. As an example, we represent the stabilizer $X_1Z_2Y_3Y_4X_5I_6$ of the $[\![6, 1, 3]\!]$ code as the vector $[1, 3, 2, 2, 1, 0]$. In a stabilizer code, we naturally have a prescription for defining four logical operators: $\{\bar{\mathsf{I}}, \bar{\mathsf{X}}, \bar{\mathsf{Y}}, \bar{\mathsf{Z}}\} \in \mathcal{L}$. These operators can be used to define logical equivalence classes, permitting us to formulate a rank-n tensor as

$$\mathsf{T}(\mathcal{L})_{\alpha_1,\ldots,\alpha_n} := \begin{cases} 1 & \text{if } P_{\alpha_1} \otimes \cdots \otimes P_{\alpha_n} \in \mathcal{SL} \\ 0 & \text{otherwise.} \end{cases} \tag{2}$$

Here, we take $\alpha_1, \ldots, \alpha_n$ to be the mapping of a given stabilizer or logical operator to $\mathbb{Z}_4$, as shown above; $P_{\alpha_1} \otimes \cdots \otimes P_{\alpha_n}$ represents the Pauli stabilizer formed from the inverse mapping, and $\mathcal{SL}$ is the logical coset of $\mathcal{S}$ with respect to $\mathcal{L}$.

As a side remark, the tensors of Eq. (2) are not, strictly speaking, isometric. However, they facilitate efficient contraction, provided that the proper index contraction sequence is indicated; as such, the full decoding process which we will describe below exhibits a runtime complexity of $O(n^{2.37})$ in the best case [53,54]. More details on the formation of large tensor networks using the aforementioned scheme can be found in [7,55].

The tensor-network decoder is a maximum-likelihood (ML) decoder, which is shown to be optimal given the error model. The ML decoder generally works by calculating the most-likely correction needed to return the system to the correct code state, given a syndrome. Here, we define a syndrome as the set $\mathbf{s} = [s_1 \cdots s_{n-k}]$ of $\mathbb{Z}_2$ parity results from measuring each stabilizer. An error E is initialized as a probability vector corresponding to each individual physical qubit; this vector is then contracted with the holographic tensor network, permitting us to calculate the syndrome $\mathbf{s} = \mathsf{HE}$, where H is the parity-check matrix of the holographic code.

After finding the syndrome, we deduce the pure error (or destabilizer) E_{pure} by taking the Moore-Penrose inverse (or pseudoinverse) $\mathsf{H}^{\dagger}_{\text{pseudo}}$ of the parity-check matrix, resulting in the equation

$$\mathsf{E}_{\text{pure}} = \mathsf{H}^{\dagger}_{\text{pseudo}}\mathbf{s}. \tag{3}$$

Once the pure error is obtained, we proceed to calculate the probability that an error with the form of E_{pure} has occurred on the n physical qubits; this is done by contracting the tensor network with tensors that parametrize the probability of errors on each physical qubit on the boundary. For independently distributed errors, even an exact contraction is efficient. From this procedure, we obtain the expression

$$\mathbb{P}(L, \mathbf{s}) := \sum_{S \in \mathcal{S}} \text{Prob}[\mathsf{E}_{\text{pure}}|SL], \quad \forall\, L \in \mathcal{L}, \tag{4}$$

where $\text{Prob}[\mathsf{E}_{\text{pure}}|SL]$ signifies the probability of a pure error acting on the coset of stabilizer $S \in \mathcal{S}$ with respect to logical operator $L \in \mathcal{L}$. In practice, the decoder must find $L \in \mathcal{L}$ such that $\mathbb{P}(L, \mathbf{s})$ is maximized, i.e., $\arg\max_{L\in\mathcal{L}}[\mathbb{P}(L, \mathbf{s})]$. As an additional condition, the summation over all logical cosets must be equivalent to unity; that is, $\sum_{L\in\mathcal{L}} \mathbb{P}(L, \mathbf{s}) = 1$. As before, we refer the reader to [7,16,55] for further details on calculating the logical success rate.

III. RESULTS

A. Noise model and setup

The error model tested in this work consists of the code-capacity error model for Pauli noise. Such an error model takes on the form

$$\mathsf{E}(\rho) = (1 - p)\rho + p(r_X X\rho X + r_Y Y\rho Y + r_Z Z\rho Z), \tag{5}$$

with the relative error probabilities $r_X + r_Y + r_Z = 1$, typically in the regime of $r_X = r_Y$ with a bias $\eta = \frac{r_Z}{r_X+r_Y} \geqslant \frac{1}{2}$ (in the case of Z-biased noise). When $\eta = \frac{1}{2}$, one recovers the standard depolarizing noise channel. If we move $\eta \to 0$, then we necessarily move towards *2-Pauli* noise; that is, noise channels consisting only of two Pauli operators, such as XZ or XY noise.

The seed tensors and their associated logical operators and their stabilizers are shown in Table I. Here we use the notation XX to denote $X \otimes X$ for brevity. Additionally, the final entry for each stabilizer generator (with a bar above) denotes the action on the logical index.

Threshold calculations were performed using the tensor-network decoder from Refs. [7,16]. These decoders and others have been made public in a software package for holographic quantum error-correction codes [56]. However, for the purposes of understanding the current work, we focus on surveying biased-noise resilience for a swath of known holographic codes, and not on a systematic treatment of tensor-network decoding methodology [53]. Threshold values were determined by computing the intersection points of the

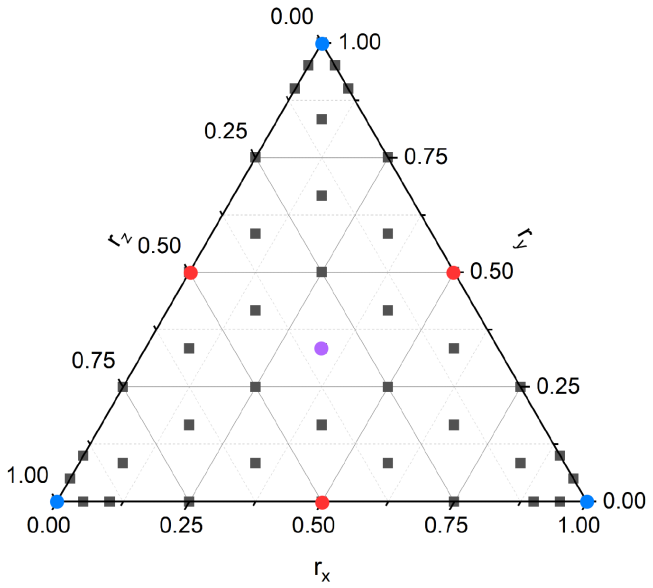


FIG. 2. Threshold data points surveyed for the holographic codes tested in this work. All data points were ascertained using four threshold crossing points at each corresponding marker in the diagram. In blue, we highlight the pure Pauli biased points, and in red, we have accentuated the 2-Pauli bias points considered in this work. The depolarizing noise point is denoted in violet.

recovery rate curves across codes at successive layers. Because these crossing points may not coincide exactly (owing to finite-size effects and Monte Carlo sampling error), we report the final threshold as the average of all such intersections, with the standard deviation serving as our measure of uncertainty.

In our biased-noise threshold profiling, we tested 43 distinct Pauli biases and have displayed them on the ternary diagram shown in Fig. 2. Each point of the triangular plot shown represents a pure Pauli error channel. Subsequently, points on the interior of the plot can be read by following the grid lines provided to the boundaries; for example, the point to the lower left of the central depolarizing noise marker can be interpreted as having relative biases $\bar{r} = (r_X,\ r_Y,\ r_Z)$ of $(0.25,\ 0.25,\ 0.5)$. At each bias point, 10 000 Monte Carlo simulations were performed per threshold curve data point, per layer. We display commensurate threshold curve results for some select data points in Fig. 4 for the zero-rate HaPPY code.

B. Zero-rate holographic code results

The ternary plots for all four zero-rate holographic codes tested in this paper are depicted in Fig. 3. From Figs. 3(a)–3(d), we have displayed the HaPPY code, Steane code, $[\![6, 1, 3]\!]$ code, and SCF. At the center of each diagram, where depolarizing noise is represented, the zero-rate HaPPY code exhibits the lowest resilience ($p_{\text{th}} = 17.9\%$), whereas all other tested codes indicate thresholds in the region $p_{\text{th}} = \approx 18\%$–$19\%$. As we move along each plot towards a pure 1-Pauli bias, we see starkly distinct behavior for every holographic code that is assessed: For example, the zero-rate HaPPY code [Fig. 3(a)] attains clear 50% thresholds in each of the pure 1-Pauli biases, while the Steane code's resilience [Fig. 3(b)] appears to decrease. In the $[\![6, 1, 3]\!]$ code and the SCF, we observe asymmetrical biased-noise profiles with respect to pure Pauli noise behavior. For the $[\![6, 1, 3]\!]$ code, we note that under pure 1-Pauli X and Y noise channels, the threshold of the code increases, albeit more slowly than for the HaPPY code; notwithstanding this similarity, the $[\![6, 1, 3]\!]$ code's threshold dips by a small amount as we move towards the pure-Z region of the ternary plot. Interestingly, the SCF also evinces an asymmetrical biased-noise threshold spectrum. However, the SCF manifests a high tolerance to pure-Y errors, but decreases with pure-X and -Z errors, as in the Steane code.

As a more detailed example, we plotted in Fig. 4 the individual threshold curves obtained for the zero-rate HaPPY code for depolarizing noise, as well as for biased pure-X, pure-Y, and pure-Z noise. Around the fixed points in Figs. 4(b)–4(d), the recovery rate promptly increases, which is due to several reasons: First, the pure 1-Pauli noise capacity can be shown to be 50%. Second, as the tensor-network decoder is a maximum-likelihood decoder, after the $p = 0.50$ mark, the decoder selects the most-probable error and returns a pure error (destabilizer) vector, which is used to correct. Therefore, unlike a minimum-weight decoder, the tensor-network decoder is still able to provide the right correction with high probability even when $p > 0.50$. More details can be found in Refs. [24,55].

If we look beyond the pure 1-Pauli portion of the ternary plots, we note a more subtle behavior of these codes: for example, it can be seen that modest threshold increases emerge for the Steane and $[\![6, 1, 3]\!]$ codes as we move towards pure *2-Pauli* noise, i.e., XY, YZ, and XZ noise. These changes can be seen more clearly by examining the threshold behavior of the codes via the tuning of a bias parameter η. In previous work, this aim was accomplished by comparing various zero-rate codes against the hashing bound, a useful lower bound for quantifying code-capacity channel performance [13]. However, in contrast to the present work, all previous works have examined the pure 1-Pauli noise limit associated with the hashing bound and have not delved into combinations of two types of Pauli errors at once, a condition known to occur in the square-lattice GKP code under a symmetric Gaussian random displacement noise channel [57–60], as well as for error channels resulting from performing Pauli twirling on the amplitude-damping noise channel [61]. As such, we tune the η parameter within the range $0 \leqslant \eta \leqslant +\infty$, extending previous work past the regime indicated by $\eta \geqslant 0.5$ [13–15].

The hashing bound is formally defined as

$$R = 1 - H(\bar{p}), \tag{6}$$

where R represents an achievable rate k/n for a random stabilizer code and $H(\bar{p})$ represents the Shannon entropy [62],

$$H(\bar{p}) = -\sum_{i\in\{I,X,Y,Z\}} p_i \log p_i. \tag{7}$$

Here, $\bar{p} = (1 - p,\ p\,r_X,\ p\,r_Y,\ p\,r_Z)$ denotes the full probability vector over the Pauli channel, where $r_X + r_Y + r_Z = 1$ as stated before, and p represents the overall physical error probability. For a given noise model, there exists a physical

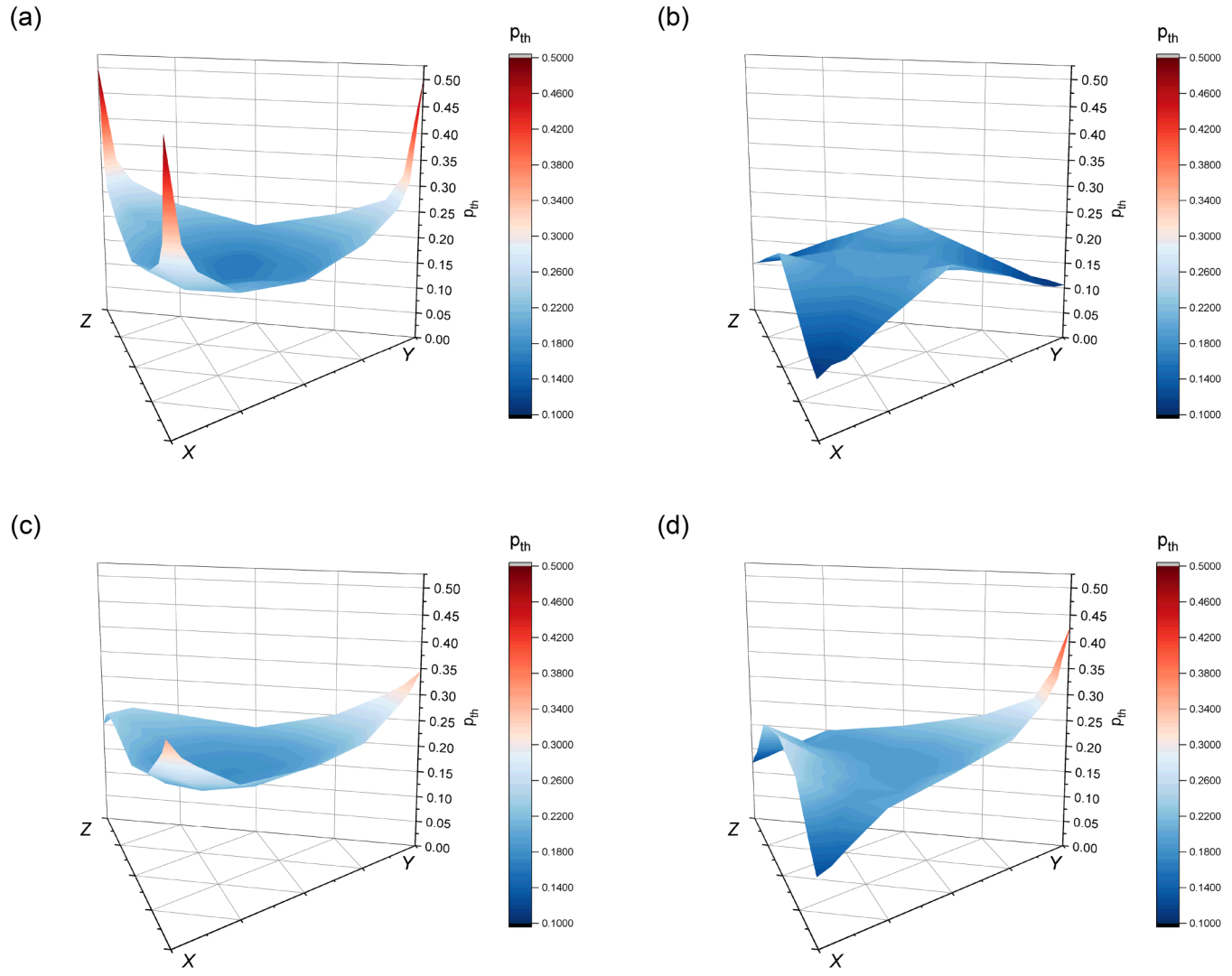


FIG. 3. Ternary plots for all holographic codes investigated in this study under biased noise, in the code-capacity setting. (a)–(d) The zero-rate HaPPY, Steane, $[\![6, 1, 3]\!]$, and SCF codes; thresholds are color coded from dark blue ($p_{\text{th}} = 10\%$) to dark red ($p_{\text{th}} = 50\%$). Additionally, we tested the tailored $[\![7, 1, 3]\!]$ code from [14,22], which achieved an identical threshold profile to that of the HaPPY code.

error probability p, at some given relative bias vector $\vec{r}$, for which the achievable rate R goes to zero. This achievable rate via random coding is known as the zero-rate hashing bound.

Figure 5 depicts the comparison of the zero-rate hashing bound for $0 \leqslant \eta \leqslant +\infty$ with all four of the surveyed zero-rate holographic codes. In our plots, we calculate physical recovery rates for the following noise biases:

$$\eta \in (0, 1/1000, 33/10000, 99/10000, 33/1000, 1/10, 1/3, 1/2, 1, 3, 10, 30, 100, 300, 1000, +\infty). \quad (8)$$

In these results, the biased-noise properties of these codes manifest themselves across the full landscape of possible pure and 2-Pauli biases, i.e., pure-X, -Y, and -Z noise, in addition to pure-XY, -YZ, and -XZ noise. In Figs. 5(a)–5(c), we illustrate the bias tuning for pure-X, -Y, and -Z biases; consequently, as we tune the parameter η in the direction towards zero, we effectively remove X, Y, and Z noise from the simulations, in effect achieving, as $\eta \to 0$, pure-YZ noise from Fig. 5(a), pure-XZ noise from Fig. 5(b), and pure-XY noise from Fig. 5(c).

Table II displays several specific threshold points of interest in the ternary plots from Fig. 3. Noise biases and their corresponding bias vectors are displayed, and figures in green and gold signify threshold data which either attain or exceed the hashing bound, or come within 2% of achieving the bound, respectively.

As is evidenced in each of the plots, the zero-rate HaPPY and tailored $[\![7, 1, 3]\!]$ codes clearly achieve the hashing bound for all pure 1-Pauli biases, as well as for finite biases in which $\eta > 10$. Additionally, in the limits for which $\eta \to 0$, the HaPPY and tailored $[\![7, 1, 3]\!]$ code thresholds closely trace out the hashing bound as pure 2-Pauli noise is approached. The behavior of the HaPPY code emulates in large part the behavior seen of the generalized toric code family [14]; we discuss this in more detail in Sec. IV.

The Steane code portrays a distinct trend: in the pure 1-Pauli noise limit, the code performs significantly worse than all other tested codes. Nonetheless, the zero-rate Steane code

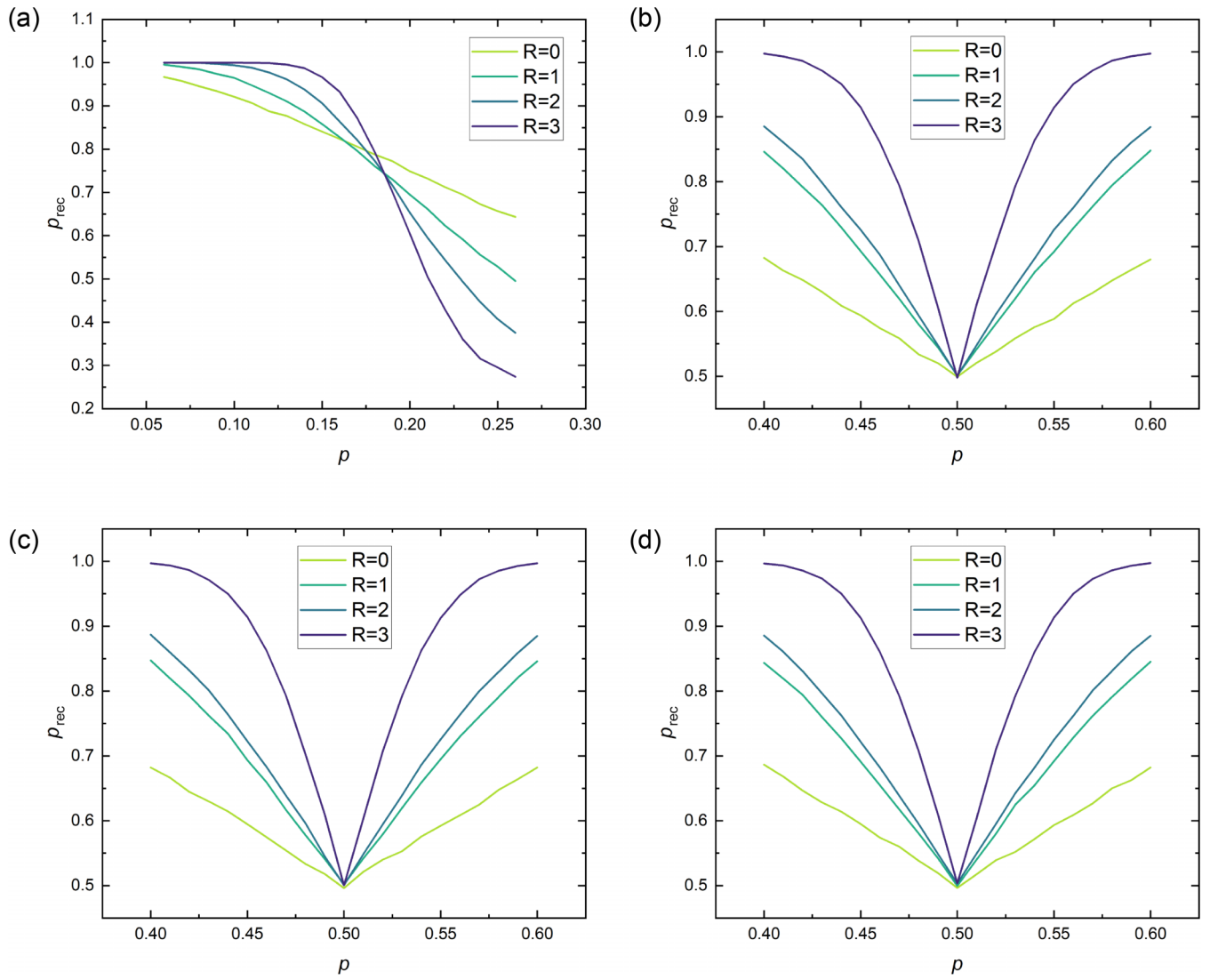


FIG. 4. Threshold curves for depolarizing, pure-X, -Y, and -Z noise, as studied using the tensor-network decoder, for the zero-rate HaPPY code at up to $R = 3$ layers of edge inflation. Here, p_{rec} represents the probability for logical qubit recovery, following from [7,9,23].

eclipses the hashing bound for depolarizing noise ($\eta = 0.5$), while also approaching the bound for finite biases as we approach the pure 2-Pauli limit ($\eta = 0$). It was shown in previous work [64] that the color code exhibits similar behavior in the pure 1-Pauli bias regime; as such, it is logical to infer that the holographic Steane code manifests similar behavior in these limits. Due to the fact that both codes are built from self-dual CSS codes [26], in the 1-Pauli limit, only one set of stabilizers gives information about the error, while the other stabilizers do not yield additional information for decoding. As such, the problem reduces to a classical linear code with a check matrix defined by only half of the symplectic check matrix in the quantum code. Notwithstanding, it is known that many code concatenation schemes based on graph states can slightly exceed the hashing bound; our results, up to the uncertainty margin given, show that the holographic Steane code can at least match most of the codes discovered in [20]. In [15,25], it was shown that randomized Clifford deformations, when applied to the surface code, can improve threshold performance with respect to a code-capacity noise channel. In this way, a surface code may be tailored to achieve the 1-Pauli hashing bound; one wonders whether such randomized approaches could be leveraged in holographic codes as well. Indeed, we may regard the additional hadamard gates in the Evenbly code [9,30] as an instance of Clifford deformation, in order to uphold the strict isometry properties present, while utilizing less highly entangled quantum states.

As a preliminary step in this direction, we have performed a random Clifford deformation of the holographic Steane code using hadamard gates, with the goal of improving the 1-Pauli threshold for the code. The seed tensors used in this modified holographic code are Clifford-equivalent to that of the original Steane code; the only difference lies in the application of hadamard gates to physical qubits 2,3,5, and 6. The resulting stabilizer generators and logical operators for this Clifford-deformed Steane code are given in Table I.

As is shown above, the stabilizers and logical operators do not follow the typical convention as expected for mixing Pauli operators in a cyclic manner, nor as in generalized toric code constructions [13–15,22]. The thresholds, reported

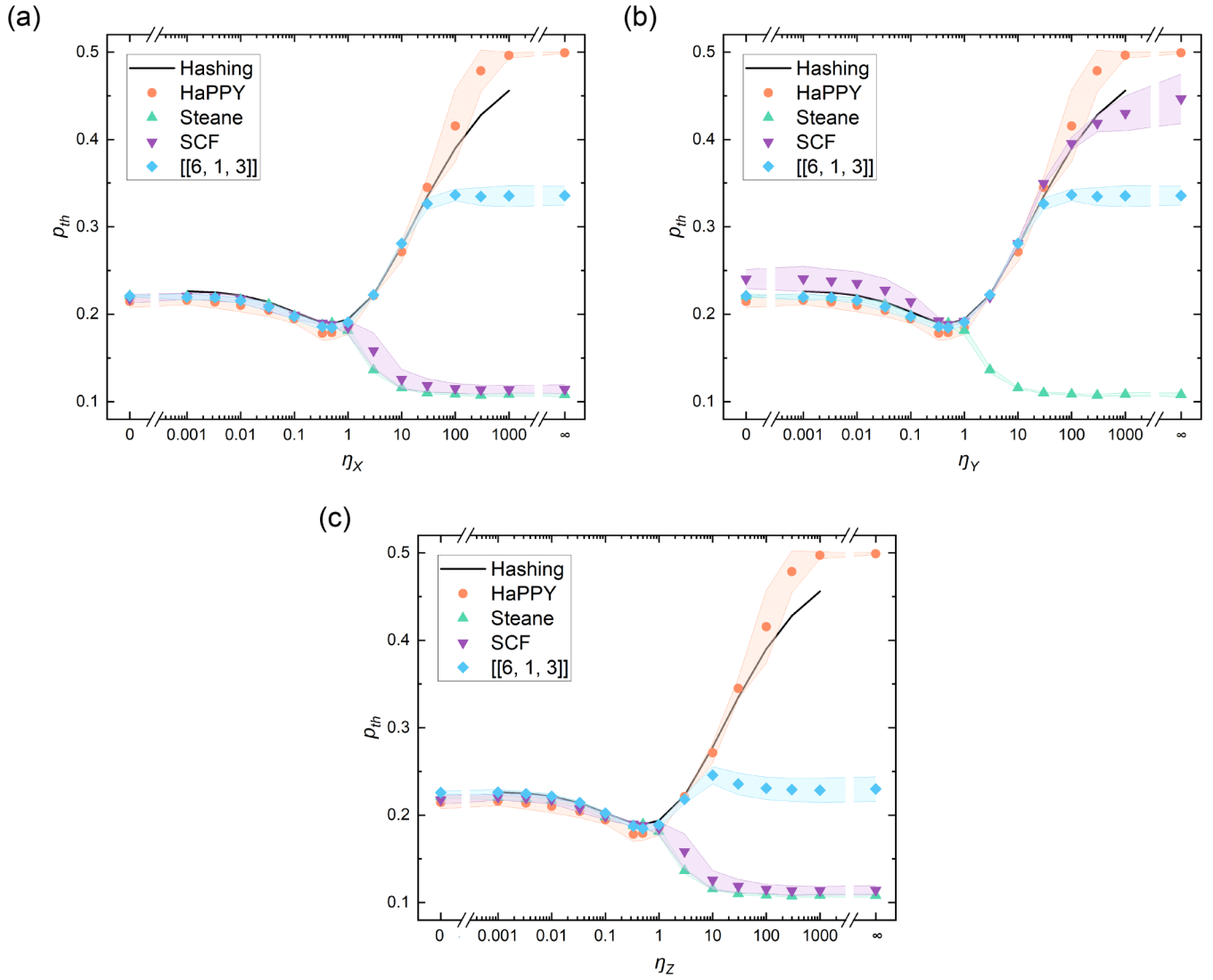


FIG. 5. Hashing bound plots for all of the codes tested in this work; we denote the hashing bound values as a black solid line, while holographic codes are shown in varying colors and markers, together with calculated uncertainties. For all of the plots, the biases range is $\eta = \{0, +\infty\}$. We list particular points of interest in Table II.

TABLE II. Recovery threshold data points p_{th} for select pure and 2-Pauli biases. The entry in blue surpasses the hashing bound, entries in green attain it up to statistical uncertainty, while entries in gold come within 2% of achieving the bound. The "HaPPY" column refers to results obtained from both the original HaPPY code of [5], as well as those from concatenating the tailored $[\![7, 1, 3]\!]$ [22]. In the last two columns, we compare to state-of-the-art results for topological codes (TQEC) as well as for graph codes: Depolarizing-noise thresholds for hexagonal color codes are taken from [63] and pure Pauli noise in surface codes from [13,64], where thresholds around the hashing bound were observed near the two-Pauli noise regime (the exact zero-bias regimes were not considered); graph code results are for the 5-in-5 code from [20].

Noise bias (r_X, r_Y, r_Z)	HaPPY (%)	Steane (%)	SCF (%)	$[\![6, 1, 3]\!]$ (%)	Hashing (%)	TQEC (%)	Graph Codes (%)
Depolarizing $(1/3, 1/3, 1/3)$	17.9 ± 0.81	18.98 ± 0.36	18.83 ± 0.13	18.46 ± 0.36	18.929	19.14	19.0597
Pure X $(1, 0, 0)$	49.92 ± 0.096	10.79 ± 0.18	11.42 ± 0.52	33.56 ± 1.08	50.00	50.00	50.00
Pure Y $(0, 1, 0)$	49.91 ± 0.11	10.8 ± 0.19	44.66 ± 2.82	33.56 ± 1.08	50.00	50.00	50.00
Pure Z $(0, 0, 1)$	49.91 ± 0.11	10.8 ± 0.19	11.42 ± 0.52	22.99 ± 1.39	50.00	50.00	50.00
Pure XZ $(1/2, 0, 1/2)$	21.45 ± 0.68	22.1 ± 0.16	24.027 ± 1.08	22.08 ± 0.04	22.709	≈Hashing	22.684
Pure XY $(1/2, 1/2, 0)$	21.45 ± 0.69	22.1 ± 0.17	21.77 ± 0.51	22.58 ± 0.17	22.709	≈Hashing	22.684
Pure YZ $(0, 1/2, 1/2)$	21.45 ± 0.68	22.1 ± 0.17	21.77 ± 0.51	22.08 ± 0.04	22.709	≈Hashing	22.684

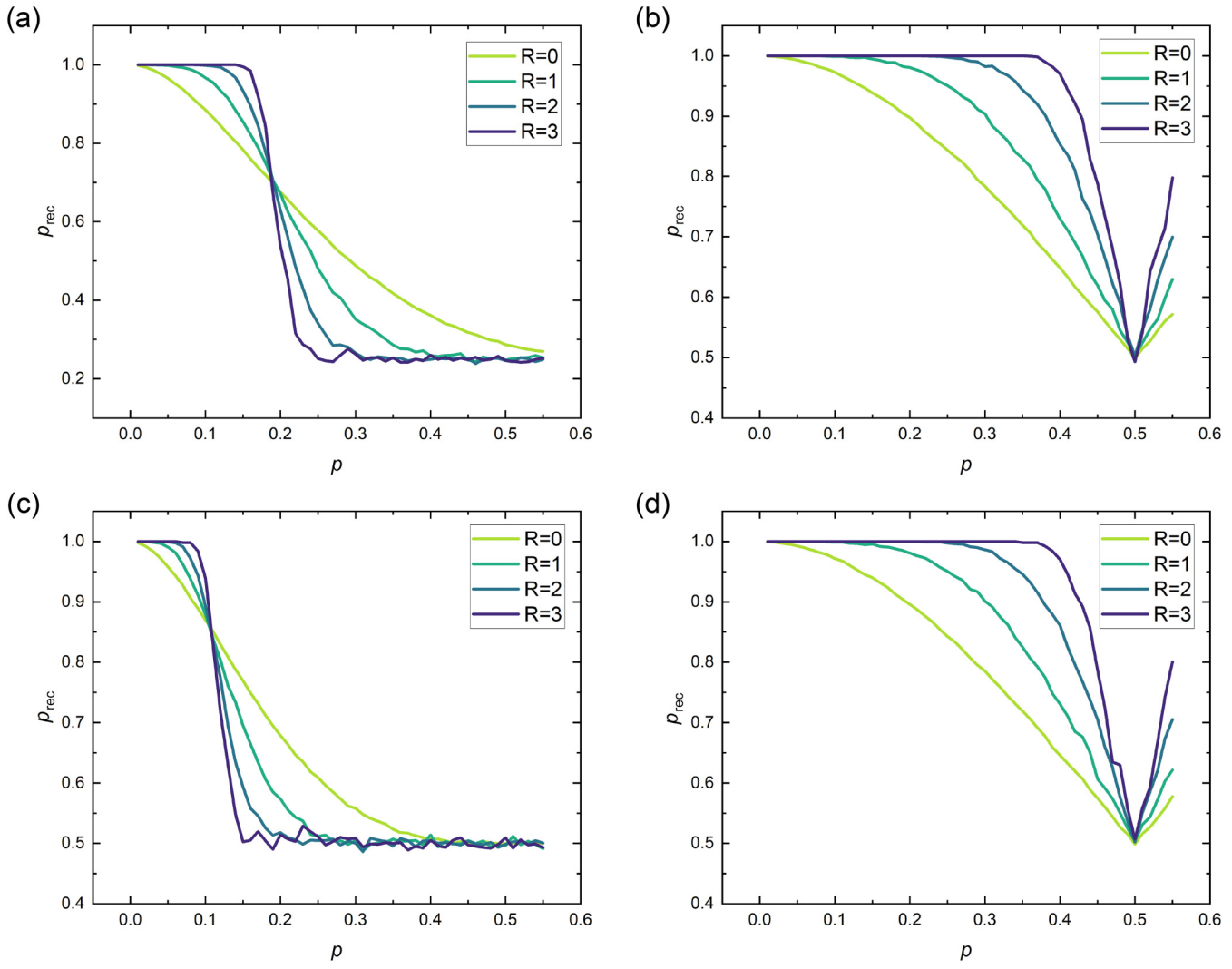


FIG. 6. Threshold curves for the Clifford-deformed Steane code that we mention in Sec. IV. Here, we have applied hadamard gates to physical qubits 2, 3, 5, and 6. In (a), we document a slight threshold increase to $19.0 \pm 0.33\%$. (b),(d) The thresholds under pure-X and -Z noise, respectively, under which an increase to approximately 50% can be observed. (c) The results for pure-Y noise, with an apparent slight decrease to $10.58 \pm 0.12\%$. As in Fig. 4, p_{rec} represents the probability for logical qubit recovery, hailing from [7,9,23].

in Fig. 6, are for (a) depolarizing noise ($19.0 \pm 0.33\%$), (b) pure-X noise ($\sim$50%), (c) pure-Y noise ($10.58 \pm 0.12\%$), and (d) pure-Z noise ($\sim$50%). We observe that even our naive Clifford deformations, when combined with the holographic concatenation method, can greatly improve the threshold performance for targeting noise models of interest. Indeed, our results show that the Clifford-deformed holographic Steane code achieves the hashing bound for pure-X and -Z noise, and supersedes the bound for depolarizing noise. Such modifications will be investigated and are the subject of active research.

The SCF displays very interesting behavior at several points in Fig. 5. For biased X and Z noise, the SCF performs similarly to the Steane code as $\eta \to +\infty$; this is due to the CSS properties of the seed tensor for both codes, as fewer parity checks are used for distinguishing errors in the limit of pure 1-Pauli noise. For biased Y noise, however, the SCF exhibits excellent threshold performance; although the SCF does not attain the hashing bound in the pure-Y noise limit, many points of finite bias reach the bound. Additionally, as we tune the parameter η back towards zero, the pure-XZ limit shows that the SCF surpasses the hashing bound at finite bias ($\eta \leqslant 0.1$). To the best of our knowledge, no other code construction thus far has surpassed the hashing bound for 2-Pauli noise [19,20].

Lastly, the $[\![6, 1, 3]\!]$ code also exhibits breakaway threshold behavior, albeit for pure-XY noise. However, it can be observed in Fig. 5 that various points within the finitely biased range $\eta \in [0, 0.5]$ either come within 2% of the hashing bound or slightly exceed it.

IV. DISCUSSION

We have presented a code-capacity study of zero-rate holographic codes under biased Pauli noise using tensor-network maximum-likelihood decoding. Across the HaPPY, tailored $[\![7, 1, 3]\!]$, Steane, $[\![6, 1, 3]\!]$, SCF, and Clifford-deformed Steane constructions, every tested code attains or exceeds the

zero-rate hashing bound for at least one bias regime. The most notable cases occur in the 2-Pauli limits: the SCF exceeds the hashing bound for XZ noise, while the $[\![6, 1, 3]\!]$ code does so for XY noise. These results indicate that holographic codes form a competitive class of efficiently decodable stabilizer codes for biased channels, beyond conventional topological-code and tree-concatenated constructions [13,15,20,21,25,64–67].

From the perspective of quantum coding theory, the relevance of these results is that holographic codes provide a structured, efficiently decodable route to thresholds near or above the random-coding hashing benchmark. The quantum channel capacity of Pauli channels is generally not known exactly, and even for the depolarizing channel there remains a gap between known lower and upper bounds [17,62,68–73]. Our results therefore add holographic generalized concatenation to the list of code-design mechanisms that can probe this gap. Unlike random stabilizer codes, however, the holographic constructions that are studied here admit tensor-network maximum-likelihood decoding with efficient exact contraction for the considered zero-rate geometries [7,11].

The observed threshold behavior suggests that hyperbolic connectivity can provide an advantage over ordinary tree-style concatenation. To check that the reported behavior is not solely a seed-tensor effect, we compared the holographic Steane construction with the corresponding tree-style concatenated Steane code built from the same ($[\![7, 1, 3]\!]$) seed tensor and decoded under the same Pauli noise model. This matched comparison isolates the role of the loopy holographic connectivity from the local Steane seed data. We find that the tree-style construction gives thresholds that are comparable in scale, but generally lower than those of the holographic Steane construction in the tested regimes. Thus, while some features of the biased-noise response are inherited from the seed tensor and concatenation structure, the comparison indicates that the loopy hyperbolic connectivity contributes a measurable threshold advantage. In a purely treelike concatenation, detection and correction remain confined to a single branch. By contrast, the hyperbolic tessellation can couple otherwise distinct branches through intermediary tensors, allowing error information to be shared across branches and increasing the set of error patterns correctable by the higher-layer seed codes. A more systematic comparison with generalized concatenated codes remains an important direction for future work.

Several extensions are immediate. First, tensor-network decoding should be applied to Evenbly-type holographic codes and their Clifford-deformed variants [9,30,74,75]. Such treatment requires incorporating edge Clifford gates directly into the decoder so that the correct destabilizers are extracted from the measured syndrome. Second, one should optimize Clifford deformations of the seed tensors for a target Pauli channel rather than using the simple hadamard deformation considered here. Third, gauge-fixing choices and logical-qubit implantation patterns should be optimized jointly with the decoder since both can change the effective threshold landscape [16,76].

We also emphasize that the zero-rate regime is not limited to the single-central-logical-qubit construction used in this paper. That setting provides the cleanest comparison with existing concatenated-code literature, but more general asymptotically zero-rate holographic families can be obtained by placing a fixed number of logical qubits on one bulk layer and then increasing the number of outer inflation layers. A punctured or annular construction, in which the central tensor is removed while a homogeneous shell of bulk logical qubits is retained, is one such example. Decoding these multilogical zero-rate codes requires a posterior distribution over multiple logical cosets, and the relevant failure metric may differ depending on whether one reports block failure or per-logical-qubit failure. A biased-noise threshold study of these multilogical zero-rate constructions is therefore a natural next step.

Finally, the practical value of biased-noise thresholds depends on whether the physical implementation preserves the bias through syndrome extraction and logical operations. Bias can be degraded by gates, measurements, and leakage mechanisms [77]. This issue is especially relevant for proposed concatenations with bosonic codes, where 2-Pauli effective channels arise naturally, for example in GKP noise models and Pauli-twirled amplitude damping [57–61,78–81]. Determining whether holographic codes can retain their biased-noise advantage under circuit-level noise is therefore the key practical question left open by this code-capacity study.

ACKNOWLEDGMENTS

We thank Aritra Sarkar, David Elkouss, and Jens Eisert for discussions related to concatenated codes and quantum channel capacity, and Sivaprasad Omanakuttan for mentioning issues related to bias preservation, principally investigated in [77]. We also thank Mackenzie Shaw and Kathleen Chang for mentioning at the conference FTQC ’24 in Benasque several realistic examples of 2-Pauli noise arising in practical quantum computing. M.S. and S.F. acknowledge financial support from the Intel Corporation. A.J. was supported by the Einstein Research Unit “Perspectives of a quantum digital transformation” and Berlin Quantum.

J.F. developed and implemented the tensor-network decoder during his master thesis, under the supervision of M.S. and S.F. M.S., C.C., and A.J. wrote the manuscript. A.J., C.C., and S.F. provided project guidance.

[1] E. Witten, Anti–de Sitter space and holography, Adv. Theor. Math. Phys **2**, 253 (1998).

[2] J. Maldacena, The large-N limit of superconformal field theories and supergravity, Intl. J. Theor. Phys. **38**, 1113 (1999).

[3] S. Gubser, I. Klebanov, and A. Polyakov, Gauge theory correlators from non-critical string theory, Phys. Lett. B **428**, 105 (1998).

[4] A. Almheiri, X. Dong, and D. Harlow, Bulk locality and quantum error correction in AdS/CFT, J. High Energy Phys. 04 (2015) 163.

[5] F. Pastawski, B. Yoshida, D. Harlow, and J. Preskill, Holographic quantum error-correcting codes: Toy models for the bulk/boundary correspondence, J. High Energy Phys. 06 (2015) 149.

[6] A. Jahn and J. Eisert, Holographic tensor network models and quantum error correction: A topical review, Quantum Sci. Technol. **6**, 033002 (2021).

[7] T. Farrelly, R. J. Harris, N. A. McMahon, and T. M. Stace, Tensor-network codes, Phys. Rev. Lett. **127**, 040507 (2021).

[8] C. Cao and B. Lackey, Quantum Lego: Building quantum error correction codes from tensor networks, PRX Quantum **3**, 020332 (2022).

[9] M. Steinberg, J. Fan, R. J. Harris, D. Elkouss, S. Feld, and A. Jahn, Far from perfect: Quantum error correction with (hyperinvariant) evenbly codes, Quantum **9**, 1826 (2024).

[10] M. Steinberg, J. Fan, J. Eisert, S. Feld, A. Jahn, and C. Cao, Universal fault-tolerant logic with heterogeneous holographic codes, arXiv:2504.10386.

[11] C. Cao, M. J. Gullans, B. Lackey, and Z. Wang, Quantum Lego expansion pack: Enumerators from tensor networks, PRX Quantum **5**, 030313 (2024).

[12] K. Sahay, J. Jin, J. Claes, J. D. Thompson, and S. Puri, High-threshold codes for neutral-atom qubits with biased erasure errors, Phys. Rev. X **13**, 041013 (2023).

[13] J. P. B. Ataides, D. K. Tuckett, S. D. Bartlett, S. T. Flammia, and B. J. Brown, The XZZX surface code, Nat. Commun. **12**, 2172 (2021).

[14] Q. Xu, N. Mannucci, A. Seif, A. Kubica, S. T. Flammia, and L. Jiang, Tailored XZZX codes for biased noise, Phys. Rev. Res. **5**, 013035 (2023).

[15] A. Dua, A. Kubica, L. Jiang, S. T. Flammia, and M. J. Gullans, Clifford-deformed surface codes, PRX Quantum **5**, 010347 (2024).

[16] T. Farrelly, N. Milicevic, R. J. Harris, N. A. McMahon, and T. M. Stace, Parallel decoding of multiple logical qubits in tensor-network codes, Phys. Rev. A **105**, 052446 (2022).

[17] D. P. DiVincenzo, P. W. Shor, and J. A. Smolin, Quantum-channel capacity of very noisy channels, Phys. Rev. A **57**, 830 (1998).

[18] G. Smith and J. A. Smolin, Degenerate quantum codes for Pauli channels, Phys. Rev. Lett. **98**, 030501 (2007).

[19] J. Fern and K. B. Whaley, Lower bounds on the nonzero capacity of Pauli channels, Phys. Rev. A **78**, 062335 (2008).

[20] J. Bausch and F. Leditzky, Error thresholds for arbitrary Pauli noise, SIAM J. Comput. **50**, 1410 (2021).

[21] S. Bhalerao and F. Leditzky, Improving quantum communication rates with permutation-invariant codes, arXiv:2508.09978.

[22] A. Robertson, C. Granade, S. D. Bartlett, and S. T. Flammia, Tailored codes for small quantum memories, Phys. Rev. Appl. **8**, 064004 (2017).

[23] R. J. Harris, N. A. McMahon, G. K. Brennen, and T. M. Stace, Calderbank-Shor-Steane holographic quantum error-correcting codes, Phys. Rev. A **98**, 052301 (2018).

[24] R. J. Harris, E. Coupe, N. A. McMahon, G. K. Brennen, and T. M. Stace, Decoding holographic codes with an integer optimization decoder, Phys. Rev. A **102**, 062417 (2020).

[25] E. Huang, A. Pesah, C. T. Chubb, M. Vasmer, and A. Dua, Tailoring three-dimensional topological codes for biased noise, PRX Quantum **4**, 030338 (2023).

[26] D. A. Lidar and T. A. Brun, *Quantum Error Correction* (Cambridge University Press, Cambridge, 2013).

[27] M. Grassl, P. Shor, G. Smith, J. Smolin, and B. Zeng, Generalized concatenated quantum codes, Phys. Rev. A **79**, 050306 (2009).

[28] L. Boyle, M. Dickens, and F. Flicker, Conformal quasicrystals and holography, Phys. Rev. X **10**, 011009 (2020).

[29] A. Jahn, Z. Zimborás, and J. Eisert, Central charges of aperiodic holographic tensor-network models, Phys. Rev. A **102**, 042407 (2020).

[30] M. Steinberg, S. Feld, and A. Jahn, Holographic codes from hyperinvariant tensor networks, Nat. Commun. **14**, 7314 (2023).

[31] C. Cao, Non-trivial area operators require non-local magic, J. High Energy Phys. 11 (2024) 105.

[32] C. Cao, J. Pollack, and Y. Wang, Hyperinvariant multiscale entanglement renormalization ansatz: Approximate holographic error correction codes with power-law correlations, Phys. Rev. D **105**, 026018 (2022).

[33] C. Cao and B. Lackey, Approximate Bacon-Shor code and holography, J. High Energy Phys. 05 (2021) 127.

[34] R. Shen, Y. Wang, and C. Cao, Quantum Lego and XP stabilizer codes, Quantum **9**, 1876 (2023).

[35] C. Cao and B. Lackey, Growing sparse quantum codes from a seed, arXiv:2507.13496.

[36] E. T. Campbell, B. M. Terhal, and C. Vuillot, Roads towards fault-tolerant universal quantum computation, Nature (London) **549**, 172 (2017).

[37] B. M. Terhal, Quantum error correction for quantum memories, Rev. Mod. Phys. **87**, 307 (2015).

[38] A. G. Fowler, M. Mariantoni, J. M. Martinis, and A. N. Cleland, Surface codes: Towards practical large-scale quantum computation, Phys. Rev. A **86**, 032324 (2012).

[39] N. P. Breuckmann and J. N. Eberhardt, Quantum low-density parity-check codes, PRX Quantum **2**, 040101 (2021).

[40] G. Anglès Munné, V. Kasper, and F. Huber, Engineering holography with stabilizer graph codes, npj Quantum Inf. **10**, 48 (2024).

[41] Z. Raissi, A. Burchardt, and E. Barnes, General stabilizer approach for constructing highly entangled graph states, Phys. Rev. A **106**, 062424 (2022).

[42] Z. Raissi, A. Teixidó, C. Gogolin, and A. Acín, Constructions of k-uniform and absolutely maximally entangled states beyond maximum distance codes, Phys. Rev. Res. **2**, 033411 (2020).

[43] W. Helwig, Absolutely maximally entangled qudit graph states, arXiv:1306.2879.

[44] N. Bao, C. Cao, and G. Zhu, Deconfinement and error thresholds in holography, Phys. Rev. D **106**, 046009 (2022).

[45] T. Jochym-O'Connor and R. Laflamme, Using concatenated quantum codes for universal fault-tolerant quantum gates, Phys. Rev. Lett. **112**, 010505 (2014).

[46] C. Chamberland, T. Jochym-O'Connor, and R. Laflamme, Thresholds for universal concatenated quantum codes, Phys. Rev. Lett. **117**, 010501 (2016).

[47] R. Laflamme, C. Miquel, J. P. Paz, and W. H. Zurek, Perfect quantum error correcting code, Phys. Rev. Lett. **77**, 198 (1996).

[48] A. Steane, Multiple-particle interference and quantum error correction, Proc. R. Soc. London Ser. A **452**, 2551 (1996).

[49] B. Shaw, M. M. Wilde, O. Oreshkov, I. Kremsky, and D. A. Lidar, Encoding one logical qubit into six physical qubits, Phys. Rev. A **78**, 012337 (2008).

[50] M. A. Nielsen and I. L. Chuang, *Quantum Computation and Quantum Information* (Cambridge University Press, Cambridge, 2010).

[51] M. Doroudiani and V. Karimipour, Planar maximally entangled states, Phys. Rev. A **102**, 012427 (2020).
[52] X.-G. Wen, Quantum orders in an exact soluble model, Phys. Rev. Lett. **90**, 016803 (2003).
[53] S. Bravyi, M. Suchara, and A. Vargo, Efficient algorithms for maximum likelihood decoding in the surface code, Phys. Rev. A **90**, 032326 (2014).
[54] F. Le Gall, Powers of tensors and fast matrix multiplication, in *Proceedings of the 39th International Symposium on Symbolic and Algebraic Computation* (Association for Computing Machinery, New York, 2014), pp. 296–303.
[55] J. Fan, Biased-noise threshold studies for holographic quantum error-correction codes, Master's thesis, QuTech, Technical University of Delft, Delft, the Netherlands, 2024.
[56] J. Fan, M. Steinberg, A. Jahn, C. Cao, A. Sarkar, and S. Feld, LEGO_HQEC: A software tool for analyzing holographic quantum codes, arXiv:2410.22861.
[57] M. H. Shaw, A. C. Doherty, and A. L. Grimsmo, Logical gates and read-out of superconducting Gottesman-Kitaev-Preskill qubits, arXiv:2403.02396.
[58] L. Hänggli, M. Heinze, and R. König, Enhanced noise resilience of the surface–Gottesman-Kitaev-Preskill code via designed bias, Phys. Rev. A **102**, 052408 (2020).
[59] A. L. Grimsmo and S. Puri, Quantum error correction with the Gottesman-Kitaev-Preskill code, PRX Quantum **2**, 020101 (2021).
[60] D. Gottesman, A. Kitaev, and J. Preskill, Encoding a qubit in an oscillator, Phys. Rev. A **64**, 012310 (2001).
[61] Y. Tomita and K. M. Svore, Low-distance surface codes under realistic quantum noise, Phys. Rev. A **90**, 062320 (2014).
[62] C. H. Bennett and P. W. Shor, Quantum information theory, IEEE Trans. Inf. Theory **44**, 2724 (1998).
[63] H. Bombin, R. S. Andrist, M. Ohzeki, H. G. Katzgraber, and M. A. Martin-Delgado, Strong resilience of topological codes to depolarization, Phys. Rev. X **2**, 021004 (2012).
[64] D. K. Tuckett, A. S. Darmawan, C. T. Chubb, S. Bravyi, S. D. Bartlett, and S. T. Flammia, Tailoring surface codes for highly biased noise, Phys. Rev. X **9**, 041031 (2019).
[65] B. Srivastava, A. F. Kockum, and M. Granath, The XYZ^2 hexagonal stabilizer code, Quantum **6**, 698 (2022).
[66] K. Tiurev, A. Pesah, P.-J. H. Derks, J. Roffe, J. Eisert, M. S. Kesselring, and J.-M. Reiner, The domain wall color code, Phys. Rev. Lett. **133**, 110601 (2024).
[67] B. Rahn, A. C. Doherty, and H. Mabuchi, Exact performance of concatenated quantum codes, Phys. Rev. A **66**, 032304 (2002).
[68] M. M. Wilde, *Quantum Information Theory* (Cambridge University Press, Cambridge, 2013).
[69] B. Schumacher and M. A. Nielsen, Quantum data processing and error correction, Phys. Rev. A **54**, 2629 (1996).
[70] B. Schumacher, Sending entanglement through noisy quantum channels, Phys. Rev. A **54**, 2614 (1996).
[71] I. Devetak, The private classical capacity and quantum capacity of a quantum channel, IEEE Trans. Inf. Theory **51**, 44 (2005).
[72] S. Lloyd, Capacity of the noisy quantum channel, Phys. Rev. A **55**, 1613 (1997).
[73] C. H. Bennett, D. P. DiVincenzo, and J. A. Smolin, Capacities of quantum erasure channels, Phys. Rev. Lett. **78**, 3217 (1997).
[74] G. Evenbly, Hyperinvariant tensor networks and holography, Phys. Rev. Lett. **119**, 141602 (2017).
[75] M. Steinberg and J. Prior, Conformal properties of hyperinvariant tensor networks, Sci. Rep. **12**, 532 (2022).
[76] A. Jahn, M. Steinberg, and J. Eisert, Holographic codes with many logical qubits (unpublished).
[77] S. Puri, L. St-Jean, J. A. Gross, A. Grimm, N. E. Frattini, P. S. Iyer, A. Krishna, S. Touzard, L. Jiang, A. Blais, *et al.*, Bias-preserving gates with stabilized cat qubits, Sci. Adv. **6**, eaay5901 (2020).
[78] C. Vuillot, H. Asasi, Y. Wang, L. P. Pryadko, and B. M. Terhal, Quantum error correction with the toric Gottesman-Kitaev-Preskill code, Phys. Rev. A **99**, 032344 (2019).
[79] J. Zhang, J. Zhao, Y.-C. Wu, and G.-P. Guo, Quantum error correction with the color-Gottesman-Kitaev-Preskill code, Phys. Rev. A **104**, 062434 (2021).
[80] M. P. Stafford and N. C. Menicucci, Biased Gottesman-Kitaev-Preskill repetition code, Phys. Rev. A **108**, 052428 (2023).
[81] K. Noh and C. Chamberland, Fault-tolerant bosonic quantum error correction with the surface–Gottesman-Kitaev-Preskill code, Phys. Rev. A **101**, 012316 (2020).